

Influence of Sn on the optical anisotropy of single-domain Si(001)

A. Astroppekakis,¹ J. R. Power,^{2,*} K. Fleischer,² N. Esser,² S. Galata,³ D. Papadimitriou,⁴ and W. Richter²

¹*Department of Chemical Engineering, National Technical University of Athens, Athens GR-15780, Greece*

²*Institut für Festkörperphysik, Technische Universität Berlin, PN6-1, Hardenbergstrasse 36, D-10623 Berlin, Germany*

³*Department of Physics, Aristotle University of Thessaloniki, Thessaloniki GR-54006, Greece*

⁴*Department of Physics, National Technical University of Athens, Athens GR-15780, Greece*

(Received 1 May 2000; revised manuscript received 13 October 2000; published 6 February 2001)

We apply reflectance anisotropy spectroscopy (RAS) and low-energy electron diffraction (LEED) to the study of Sn deposited on a single-domain vicinal Si(001) sample. Large variations in RAS are recorded when up to 5 monolayers (ML) of Sn is deposited on the Si substrate at room temperature. We observe (2×2) and (1×1) LEED patterns for the 0.5-ML and 1.0-ML Sn covered surfaces, respectively. The (1×1) LEED pattern exists beyond this coverage and up to 5.0-ML deposition. Even though a (1×1) LEED pattern is observed upon deposition of 1.5 ML, surprisingly, a significant optical anisotropy is observed. After annealing to 570 °C for 2 min, we observe a progression of LEED pattern changes from $c(4\times 4)\rightarrow(6\times 2)\rightarrow c(8\times 4)\rightarrow(5\times 1)$ with increased Sn coverage up to 1.5 ML. Similar RAS line shapes are obtained for all reconstructions produced through annealing with the exception of the (5×1) . For the (5×1) phase, a significant anisotropy appears in the region of 1.8 eV. Similarities in the RAS line shape for both the (5×1) phase and that obtained after deposition of 1.5 ML of Sn at room temperature may indicate a RAS sensitivity to Sn dimer orientation within the uppermost layer.

DOI: 10.1103/PhysRevB.63.085317

PACS number(s): 78.40.Fy, 07.78.+s, 73.20.At

I. INTRODUCTION

The group-IV elements Sn and Pb are examples of nonsoluble forming elements that display negligible solid solubility, resulting in abrupt interfaces when they are deposited on clean Si surfaces. Such systems can be considered representative of unreactive epitaxial interfaces and act as model systems for Schottky barrier studies.¹⁻³ Sn, in particular, can also be used as a surfactant for the growth of high-quality thin Ge layers on Si(001), making the Sn/Si interface of interest from several points of view.^{4,5}

The adsorption of monolayer coverages of Sn has been widely studied by a variety of surface-science techniques. Initial studies have shown that upon deposition of up to 1.5-monolayers (ML) of Sn (where 1 ML = 6.78×10^{14} atoms/cm²) followed by annealing to above 500 °C, a wealth of different reconstructions exist, from (2×1) , $c(4\times 4)$, (6×2) , $c(8\times 4)$, to (5×1) with increased Sn coverage.^{1,6,7} Photoemission and inverse-photoemission studies have been carried out on each of these reconstructions and surface electronic-structure information has been obtained.^{8,9} Scanning tunneling microscopy (STM) has also been applied to this system, revealing stripelike structures and trenches for the $c(4\times 4)$, (6×2) , and $c(8\times 4)$ reconstructions.¹⁰ These reconstructions, which are stabilized with increasing Sn coverage, have been interpreted in terms of varying amounts of mixed Sn-Si dimers and Sn-Sn dimers, the lower coverage $c(4\times 4)$ reconstruction possessing mostly mixed dimers while the higher coverage $c(8\times 4)$ phase comprises mainly buckled Sn-Sn dimers.¹⁰ A dimer model involving Sn dimer termination has also been proposed for the (5×1) surface. Based on STM data, the (5×1) reconstruction can be considered to consist of 0.5

ML of Sn dimers grown on an underlying monolayer of Sn dimers.^{10,11}

In this work we use low-energy electron diffraction (LEED) and reflectance anisotropy spectroscopy (RAS) to explore these Sn-induced reconstructions. RAS was developed in its present form by Aspnes and co-workers¹² and has proven to be a powerful tool for observing surface-related optical anisotropy and growth transience under both ultrahigh-vacuum¹³⁻¹⁶ (UHV) and atmospheric pressure conditions.^{17,18} The technique derives its surface sensitivity from measurements of the difference in normal-incidence reflectance for light polarized along two major orthogonal axes of the surface of cubic crystals that have isotropic bulk optical properties. In recent years, significant progress has been made in the theoretical understanding of the origins of the RAS signal from clean Si surfaces and after adsorption of various elements on Si surfaces.^{14,16,19}

By using vicinal Si(001) samples, an anisotropic surface can be produced, which is necessary for applying RAS to this system. On-axis Si(001) comprises equal proportions of two Si dimer terminated domains, differing only in the orientation of the Si dimer bonds of the surface reconstruction, which are orthogonal with respect to one another. Although in isolation each of these domains is anisotropic, the RAS signal, which averages over many domains, is zero because the signal from one domain cancels that of the other. In contrast, for vicinal Si(001) cut 4° off the [001] direction towards [110], a surface comprising predominantly one domain separated by double atomic height steps is stabilized, giving rise to a nonzero RAS signal. Upon deposition of Sn on this vicinal surface, similar RAS line shapes are obtained for all reconstructions reported previously, with the exception of the (5×1) reconstruction, where a large anisotropy in the region of 1.8 eV is observed. We interpret the possible

origin of this feature through reference to previous work.^{8–10} Finally, comparison of RAS data obtained for the (5×1) reconstruction with room-temperature RAS data is consistent with similarities in surface local structure on both surfaces.

II. EXPERIMENT

The experiments were carried out in an UHV chamber with a base pressure of 8×10^{-11} mbar. The Si substrate was *n*-type, phosphorus-doped with a resistivity in the region of $20 \Omega \text{ cm}$ and was polished 4° off the $[001]$ direction towards $[110]$. The vicinal Si(001) samples were degassed to 600°C overnight before being cleaned by sequential direct heating to 970°C while maintaining the pressure below 5×10^{-10} mbar. Sample temperature was measured either by thermocouple or by optical pyrometry. After cleaning, LEED revealed a split-spot largely single domain (1×2) pattern indicative of a dimerized surface with a regular arrangement of double atomic height steps (or *D* steps). A $(1 \times 2):(2 \times 1)$ domain ratio of 3:1 was estimated from intensity analysis measurements of the LEED half-order spot intensities.

Sn was evaporated from a miniature Knudsen cell (*K* cell) evaporator, which was calibrated by measuring island thicknesses for thick Sn layers deposited on a Si sample using an atomic force microscope (AFM).²⁰ An approximate deposition rate of 1 ML every 60 sec was extracted by this method. Sn was deposited onto the clean Si(001) samples at room temperature and the samples were annealed to 570°C for 2 min. Once both the room temperature and annealed surfaces for a particular coverage were investigated with LEED and RAS, the Sn was desorbed and a different Sn coverage was subsequently deposited. After annealing, the samples were allowed to cool down to room temperature before data acquisition.

The RAS spectrometer was directed at the sample through a strain-free optical viewport. The RAS experimental arrangement used in this work has been described elsewhere.^{12,21} The reflectance difference signal ΔR is normalized to the average reflectance *R* and is related to the surface and bulk dielectric function components by

$$\frac{\Delta R}{R} = \frac{8\pi}{\lambda} \text{Im} \left[\frac{(\epsilon_{xx} - \epsilon_{yy})d}{\epsilon_b - 1} \right], \quad (1)$$

where *d* is the thickness of the anisotropic surface layer, λ is the wavelength of light, ϵ_{xx} and ϵ_{yy} are the surface dielectric function tensor components, and ϵ_b represents the isotropic bulk dielectric function. In the present geometry, the *x* crystallographic axis is the surface $[\bar{1}10]$ direction (parallel to the step edges) while the *y* crystallographic axis is $[110]$ (perpendicular to the step edges). It follows from Eq. (1) that when ϵ_b is predominantly real, a positive signal indicates preferential absorption in the *x* direction. Equation (1) is valid only for $d \ll \lambda$. It should be noted that the quantity *d* does not simply measure the thickness of the top surface atomic layer of a clean surface or the thickness of an adsorbed overlayer. For Si(001), where the bulk optical anisotropy is zero, *d* is the thickness that contributes to the optical anisotropy, which is not only the topmost surface layers but

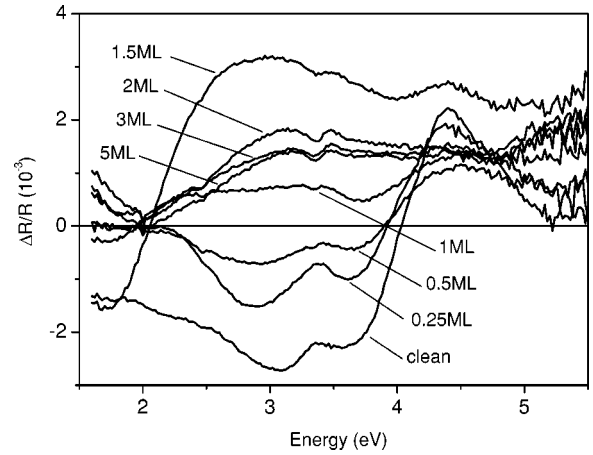


FIG. 1. (a) RAS spectra obtained by depositing various Sn coverages between 0.25 ML and 5 ML onto the clean vicinal Si(001) surface at room temperature.

also the deeper layers that are also affected by the presence of the surface or of the Sn overlayer. As ϵ_{xx} and ϵ_{yy} are also nonzero over this thickness, it becomes clear that RAS does not merely measure the optical anisotropy of the surface but rather the surface-induced optical anisotropy (SIOA). The SIOA is expressed by $(\epsilon_{xx} - \epsilon_{yy})d$.

III. RESULTS AND DISCUSSION

A. Room-temperature deposition

Figure 1 shows RAS spectra for increasing amounts of Sn deposited onto the clean Si(001) substrate at room temperature. The intensity and line shape for the clean vicinal Si(001)- (1×2) surface is in agreement with previous work.^{13,14,22} A trough at 3.0 eV exists, which has been shown recently to arise from anisotropy involving rebonding at *D* steps of vicinal Si(001) surfaces.²² The slightly shallower trough at 3.7 eV was assigned to anisotropy involving the Si dimer terminated (1×2) terrace structure.²² Hence, care must be taken in interpreting features in these RAS data as the changes observed may be either step or terrace related.

From Fig. 1, it is clear that deposition of Sn has a large effect on the surface-induced optical anisotropy, which is maximized for a coverage of 1.5 ML. Above and below this coverage, the amplitude of the RAS signal is significantly smaller. From LEED, the reconstruction changes from $(1 \times 2) \rightarrow (2 \times 2) \rightarrow (1 \times 1)$ with increasing Sn coverage up to 5.0 ML, the (2×2) saturating at 0.5 ML coverage. Initial deposition of 0.25 ML of Sn causes a significant reduction in RAS amplitude, but the line shape is similar to that of the clean surface. However, there are two notable exceptions: The trough at 3.0 eV for the clean surface has shifted downwards in energy to 2.8 eV, while the terrace-related 3.7 eV peak has become more pronounced (see Fig. 1). LEED for this surface reveals a split-spot (1×2) pattern similar to the clean surface, although with a higher background indicating some surface disorder.

Upon adsorption of 0.5 ML of Sn, a further decrease in the RAS intensity occurs and a (2×2) LEED pattern is ob-

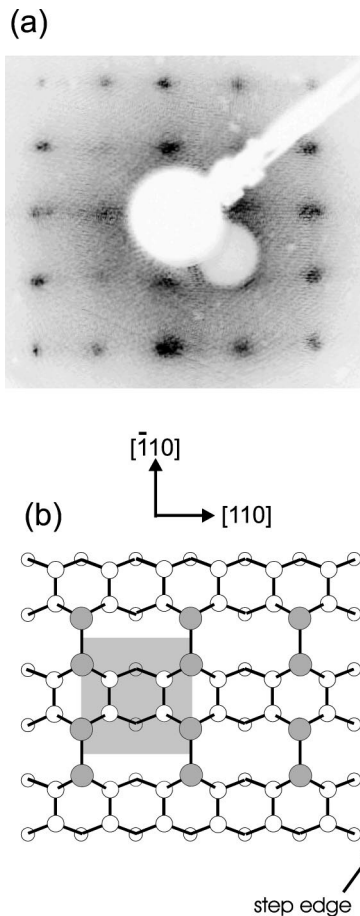


FIG. 2. (a) LEED image, taken at 51.7 eV, for the Sn-induced (2×2) phase formed at 0.5 ML, and (b) model of the (2×2) phase. Shaded area indicates the 2×2 unit cell.

served [see Fig. 2(a)]. When 1 ML of Sn has been deposited, the optical anisotropy above 2.0 eV becomes wholly positive but rather featureless, while below 2 eV, a small trough has developed (see Fig. 1) and a (1×1) LEED pattern is observed. However, deposition of 1.5 ML of Sn causes the most dramatic effect on the RAS line shape and intensity. Below 2.0 eV, a large negative trough has developed that is centered at 1.8 eV, while above 2.0 eV, a significant broad and positive feature centered near 3.0 eV and a smaller one at 4.25 eV can be seen. Subsequent deposition results in an overall reduction in the RAS signal, where both the 1.8-eV trough and 4.25-eV peak disappear, and the broad 3.0-eV structure is reduced in amplitude and shifted slightly to higher energy.

In order to interpret these results, we refer to the detailed STM work of Glueckstein *et al.*, which describes deposition of monolayer amounts of Sn onto flat Si(001) samples at room temperature.²³ In this work, a (2×2) phase has also been observed using LEED but not until *above* a coverage of 0.5 ML. The similarity of this reconstruction to the (2×2) reconstruction obtained by deposition of group-III metals on Si(001) has been suggested.^{24,25} Although a perpendicular and parallel dimer model have both been proposed for the group-III metal-induced (2×2) phase, recent work has shown that the parallel dimer model may be more

appropriate.²⁵ If this model is applicable to Sn, then each Sn dimer would bridge two underlying Si dimer rows, so that the Sn dimerization direction is oriented parallel to the dimerization direction of the underlying Si dimers [see Fig. 2(b)]. Such a parallel dimer structure would be expected to reduce the effect of strain as the Si dimer and Sn dimer compressive/tensile strains are orthogonal. Recent work on the chemically similar element Pb adsorbed at room temperature onto Si(001) has reported such a parallel dimer model, with the addition of some Pb dimer buckling.²⁶

At 0.5-ML coverage, Glueckstein *et al.* observed significant surface disorder by STM and no (2×2) LEED pattern could be distinguished. The buildup of strain associated with the 20% difference in lattice constant between α -Sn and Si (6.49 Å as opposed to 5.43 Å) was seen to cause the Sn dimer chains associated with (2×2) local order to shift laterally, that is, in a direction perpendicular to the chains, thus destroying any long-range order and ruling out the possibility of observing a (2×2) LEED pattern at 0.5-ML Sn coverage.²³ However, they argue that *above* 0.5-ML coverage, a weak (2×2) LEED pattern can be observed that is associated with the nucleation of second-layer Sn dimers. From our accurate determination of coverage, we observe a (2×2) LEED pattern at 0.5-ML coverage that would appear to be in contrast to the interpretation of Glueckstein *et al.*²³

In order to explain this, we note that in contrast to Glueckstein *et al.*, we have used a vicinal rather than a singular Si(001) sample.²³ Clean vicinal Si(001) samples contain a regular array of steps and terraces. These steps are either of single atomic height (*S*) or double atomic height (*D*) or a mixture of the two step heights, depending on the miscut angle from the (001) plane off towards $[110]$. Above a critical offcut angle of 1.3° , *S* steps become energetically unfavorable due to repulsion between neighboring steps.²⁸ The transformation of two *S* steps into one *D* step occurs and the doubling of the step height also forces the terrace to double in width, thus reducing the step repulsion and preserving the overall vicinal angle. At miscuts greater than 2° , most of the steps are thought to have undergone this transformation.²⁸

Two types of *D* step and two types of *S* step exist depending on the orientation of the Si dimer bond on the upper terrace of the step edge. For steps with the Si dimer bond on the upper terrace oriented parallel to the step edge, the subscript *B* is used; for Si dimers perpendicular to the step, the subscript *A* is used.²⁷ It has been found that S_A , S_B , and D_B steps all have similar formation energies, while D_A steps are energetically less favorable, showing a formation energy that is approximately three times higher.²⁷ While the orientation of the Si dimer bond on the upper and lower terraces of an *S*-type step edge changes, that is, the domain type changes, the orientation of the Si dimer bond (or domain type) across *D*-type steps remains the same. Hence, due to observation of the minor (2×1) domain on the samples used in this work, it is clear that this also implies the presence of *S* steps. This seems surprising as Pehlke and Tersoff have outlined that for such a 4° miscut, no *S* steps should remain.²⁸ However, if one simply calculates the terrace width at which *S* steps should become unfavorable, using the angle of 1.3° and an *S*-step height of 1.36 Å, an approximate value of 60 Å is

found, which is not a significantly larger width than the perfect 4° offcut Si(001) sample step separation of 39 Å. Considering that the theoretical study of Pehlke and Tersoff ignored the effect of temperature on step formation, it is conceivable that the elevated temperatures used in this work to clean the sample, along with the fact that the steps are not straight but meander, may allow terraces greater than 60 Å in width to form locally. The presence of such wide areas locally provides a mechanism through which S steps, and hence the minor (2×1) domain, can be stabilized and explains the presence of some of the minor domain evident in our LEED pattern.

Assuming that the deposited Sn does not affect the step structure in any way, upon formation of the Sn-induced (2×2) phase, the Sn dimer chain length formed on each of the original (1×2) terraces can only be approximately four to five Sn dimers in length before a step is reached [see Fig. 2(b)]. From previous work, steps can be considered stress domain boundaries.²⁹ Hence, within such terraces, the buildup of strain that Glueckstein *et al.*²³ have reported cannot occur as the Sn chains reach a stress domain boundary (i.e., a step) before the strain associated with the Sn dimer chains becomes critical. In the minor (2×1) terraces, there is no impediment to the formation of long Sn-induced (2×2) chains, and so the strain-induced lateral displacement of Sn-Sn dimers described by Glueckstein *et al.* is expected. However, as the clean surface is dominated in terraces of (1×2) type, it is clear that the alleviation of strain within the Sn-induced (2×2) phase formed on these terraces due to the presence of steps plays a significant role in allowing observation of the (2×2) at 0.5-ML coverage.

Upon further deposition of Sn, STM images display an increasingly complex surface structure. By 1.1-ML coverage, a second Sn layer is complete.²³ A third Sn layer commences forming at a coverage of 1.5 ML, which is complete by 1.9 ML, whereafter, the growth of irregular three-dimensional metal islands occurs.²⁵ Referring to Fig. 1, we see that deposition of 1.5 ML of Sn produces a large anisotropy signal. A weak (1×1) LEED pattern with a high background is obtained indicating no significant long-range ordering. Hence, the RAS signal that we observe must be connected with a particular local ordering in the surface. We return to a discussion of this in Sec. III C. Above 1.5-ML deposition, a reduction in RAS signal amplitude is observed that saturates at 2.0-ML coverage.

B. After annealing to 570 °C/2 min

In this section, we discuss the RAS line shapes obtained when the samples are annealed after room-temperature deposition of Sn. We separate the discussion into three subsections depending on Sn coverage.

1. Coverages below 1 ML of Sn

In Fig. 3(a), the RAS line shapes for the $c(4 \times 4)$, (6×2) , and $c(8 \times 4)$ reconstructions, which are stabilized between 0.2–0.35 ML, 0.35–0.5 ML, and 0.5–1.0 ML Sn coverage, respectively, are displayed.⁷ LEED images for the $c(4 \times 4)$ and $c(8 \times 4)$ reconstructions are shown in Fig. 4(b)

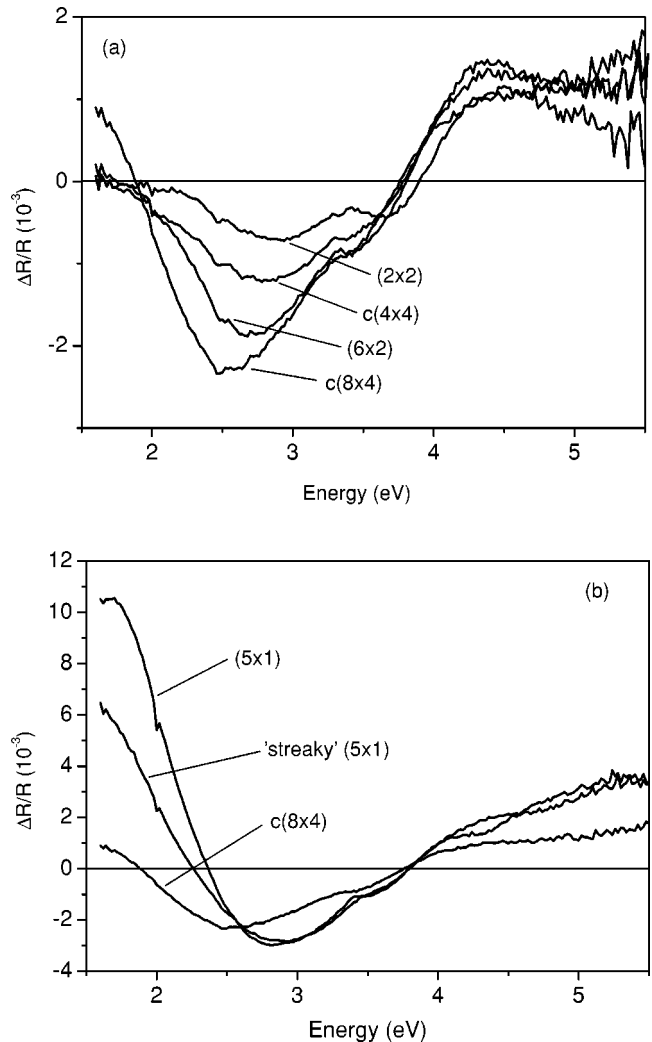


FIG. 3. RAS spectra obtained after annealing the as-deposited Sn surfaces to 570 °C for 2 min. The samples were allowed to cool down to room temperature before data acquisition. (a) Shows the RAS spectra for the $c(4 \times 4)$, (6×2) , and $c(8 \times 4)$ reconstruction, together with the room-temperature (2×2) reconstruction for comparison. (b) Shows the RAS spectra corresponding to the 1.5 ML (5×1) and higher coverage (2.0 ML) “streaky” (5×1) LEED pattern. Also shown in (b) is the $c(8 \times 4)$ phase for comparison with the RA amplitudes shown in (a).

and Fig. 4(c). It is clear from Fig. 3(a) that all line shapes show a striking similarity. To explain the origin of these similarities, we refer to previous work. Baski *et al.* have carried out detailed STM measurements of all three surfaces.¹⁰ Both the $c(4 \times 4)$ and (6×2) phases consist of missing Si dimer trenches and stripelike structures that grow perpendicular to the Si dimer rows: The higher the Sn coverage, the greater the thickness of the Sn stripes.¹⁰ The similarity of both these reconstructions has also been pointed out through the angle-resolved photoemission (ARUPS) and inverse-photoemission spectroscopy (IPES) work of Pedio *et al.*^{8,9} The ARUPS data displayed a distinct nondispersing surface state, at 0.8 eV below the Fermi level on both surfaces. Due to the lack of structural models available for these reconstructions, however, the origin of this state was not dis-

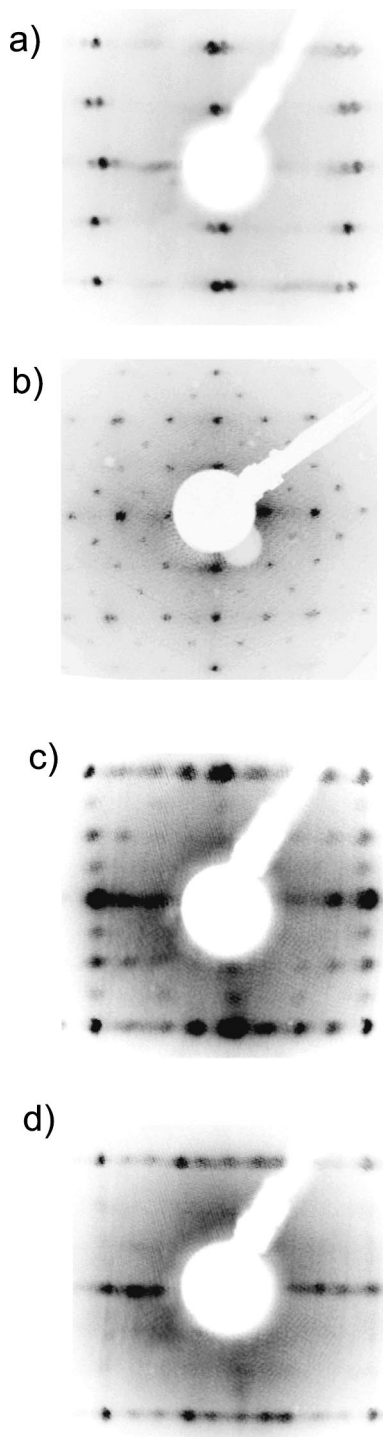


FIG. 4. LEED patterns for (a) clean Si(001)-(1 \times 2) (56.3 eV), and (b) $c(4\times 4)$ (61.8 eV), (c) $c(8\times 4)$ (56.7 eV), and (d) (5 \times 1) (55 eV) reconstructions obtained by depositing 0.25 ML, 1 ML, and 1.5 ML of Sn, respectively, at room temperature followed by annealing to 570 $^{\circ}$ C for 2 min.

cussed. In the IPES work of Pedio *et al.*,⁸ the $c(4\times 4)$ reconstruction was not observed. However, for the (6 \times 2) reconstruction, an empty surface state was found at 1.8 eV above the Fermi level. Assuming the symmetry of these surface states is such as to allow an optical transition, then such

a transition would occur at approximately 2.6 eV. From the RAS data for the (6 \times 2) reconstruction, a feature centered near 2.7 eV is observed, which is consistent with these photoemission data [see Fig. 3(a)].

With increasing Sn coverage up to 1 ML, it is likely that the shift in energy position of the RAS feature in the 2.5–3.0-eV region is related to the gradual change of mixed Sn-Si dimers [which saturate upon completion of the (6 \times 2) reconstruction] to Sn-Sn dimers, which is complete when the $c(8\times 4)$ phase is formed at 1-ML coverage.¹⁰ A gradual increase in RAS intensity is also observed up to 1-ML coverage, which is probably due to increased ordering of Sn on the surface. It should be noted that in this coverage regime, a replacement mechanism rather than the formation of a Sn adlayer is likely, as up to 1-ML coverage, the LEED 4 \times , 6 \times , and 8 \times periodicities are all along the [110] direction. This indicates that the Sn dimers should be oriented parallel to the underlying Si dimers.¹⁰ However, above 0.5 ML coverage, adlayer dimers would be expected to be oriented in the perpendicular direction. We propose that in the 0.5-ML coverage regime, one Si atom of each Si dimer must be replaced by one Sn atom, and thereafter the second Si atom is replaced. Such a replacement mechanism from low to high coverage is also consistent with an increase in amplitude as the Sn coverage increases. Once replacement takes place, the question arises as to what happens to the Si atoms that have been replaced. We return to a discussion of this point in the next section.

Comparing the RAS line shapes for these low Sn coverages with the (2 \times 2) phase formed with 0.5 ML of Sn is deposited at room temperature [see Fig. 3(a)], it can be seen that the overall line shape is similar to those obtained for the $c(4\times 4)$ and (6 \times 2) phases, with two small differences: (i) a deeper trough exists at 3.7 eV relative to the overall line shape than in the other surfaces and (ii) the energy of the low-energy trough is near 2.8 eV, which is 0.2 eV higher than that obtained for the annealed phases. A deeper trough at 3.7 eV is expected because the (2 \times 2) phase comprises no unbroken terrace Si dimers, and so such feature, which has previously been related to structure on the dimerized clean Si(001) surface, should still exist.²² The trough is smaller after annealing as Si dimer bonds are broken in favor of mixed Sn-Si dimer formation, and also trenches are formed.¹⁰ To date, no ARUPS or IPES experimental data, nor any calculated data, exist for the (2 \times 2) phase, making further interpretation of the origin of the 2.8-eV feature impossible.

2. 1-ML coverage: The $c(8\times 4)$ phase

When 1 ML of Sn is deposited on our single-domain Si(001) sample and the sample is then annealed, a $c(8\times 4)$ LEED pattern as shown in Fig. 4(c) is observed. This agrees with the results of several authors, where flat Si(001) samples were used.^{1,6–10} However, assuming no reorganization of the clean Si step structure upon Sn deposition, this reconstruction may not have been expected on our vicinal sample. As we have already outlined, the 4 $^{\circ}$ offcut vicinal Si(001) sample used in this work is dominated by terraces that are 39 \AA in width separated by D steps. A small number of larger terraces of the minority domain are also present,

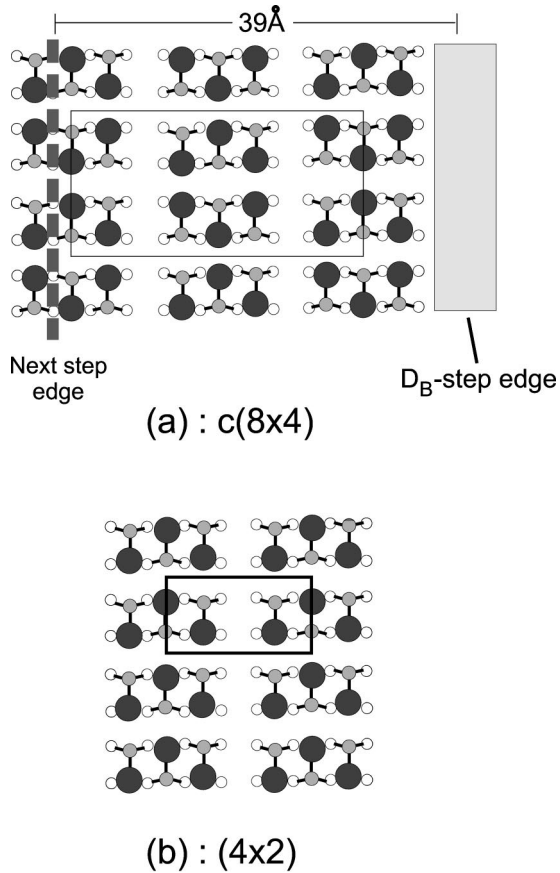


FIG. 5. Models for (a) the $c(8 \times 4)$ reconstruction (after Baski *et al.*, Ref. 9) and (b) the (4×2) reconstruction, which may coexist on narrower terraced regions of our stepped surface. In (a), the shaded area represents the area of a rebonded D_B step edge, while the dotted line represents the position of the next D_B step. The shaded atoms correspond to asymmetric Sn dimers, where each ‘up’ atom is represented by a larger circle with darker shading.

which we ignore for the moment. For the formation of the $c(8 \times 4)$ on the majority domain, the $8 \times$ periodicity, which is observed along the $[110]$ direction [see Fig. 4(b)], must comfortably fit within this 39 \AA -wide terrace in order to be able to form. This $8 \times$ periodicity or $8a$, where $a = a_0 / \sqrt{2} = 3.84 \text{ \AA}$ is the unit cell width, is 30.72 \AA . On first glance, therefore, the $c(8 \times 4)$ phase should easily be accommodated within these 39 \AA -wide terraces. Upon observation of Fig. 5(a), which is the generally accepted model of the $c(8 \times 4)$ phase, it is evident that three complete chainlike structures must fit onto one terrace in order for the $c(8 \times 4)$ phase to exist. Therefore, the terrace width needs to be an extra $2a$ wider, setting the overall terrace width required at 38.4 \AA . Although this value is just less than the 39 \AA width of the 4° offcut clean vicinal Si(001) sample, accommodation of the $c(8 \times 4)$ may still not have been expected as this 39 \AA terrace width ignores the fact that the steps on the vicinal sample also contribute to the surface area. The double height steps that dominate the step structure of such a 4° offcut Si(001) sample are known to be rebonded, making the step contribution to the surface area for such samples in the region of 20% [see Fig. 5(a)]. Hence observation of the $c(8$

$\times 4)$ phase on these terraces of our 4° offcut Si(001) samples may not have been expected. We point out that no such restrictions to the formation of the $c(8 \times 4)$ are expected on the terraces of the minor domain as the orthogonal orientation of this domain ensures that the $c(8 \times 4)$ can form, unhindered by the presence of steps.

In the preceding section, we outlined that the reconstructions formed through annealing submonolayer coverages of Sn result in Si dimer atoms being replaced with Sn. We propose that the Si that has been removed is accommodated at the D steps of the vicinal sample, extending some terraces, so that the $c(8 \times 4)$ phase can be accommodated. The lengthening of some terraces will inevitably lead to the shortening of other terraces. On shorter terrace widths, it is presumed that the $c(8 \times 4)$ phase will not form. However, if the dimer buckling within the middle chain of the $c(8 \times 4)$ structure is simply phase-shifted so that all chains are in phase, then a smaller (4×2) structure can be formed [see Fig. 5(b)]. It should be noted that in the experiments, LEED did not exclusively yield a $c(8 \times 4)$ pattern. Occasionally, a (4×2) structure was observed. This indicates that although the phase shift required to produce the (4×2) may increase the surface energy, some compensation effects are provided by the presence of steps, making this reconstruction energetically favorable.

Next, we compare the RAS line shapes for the $c(8 \times 4)$ phase with the electronic bandstructure measurements of Pedio *et al.*^{8,9} [see Fig. 3(a)]. From the figure, it can be seen that the dominant feature in the RAS response is the broad trough centered at 2.5 eV. For the $c(8 \times 4)$ phase, three surface states have been observed: S_1 , a Sn dangling-bond derived state; S_2 , Sn-Si backbond associated; and S_3 , which is related to the bond between two ‘up’ Sn atoms of adjacent dimers parallel to the chain length.⁹ S_1 and S_2 appear at 1.0 eV and approximately 1.5 eV below the Fermi level, respectively, while S_3 shows broad dispersion between 1.5 eV and 3 eV. The IPES data for the $c(8 \times 4)$ phase display only one pronounced empty state at 1.1 eV, which is associated with Sn-Sn empty and interacting dangling bonds, while another broad state exists near 2.5 eV above the Fermi level.⁸ Assuming again that transitions can exist between these states, three possible optical transitions exist, one at 2.1 eV, one at 2.6 eV, and a broad structure that may be expected from 2.6 eV to 4.1 eV. From our RAS spectra, we see some structure at 2.5 eV while nothing is observed at 2.1 eV, suggesting that either the symmetry of the states involved is wrong, or that the transition itself shows no directionality and hence is inaccessible to RAS, which relies on anisotropies in the surface electronic structure. We associate the trough in the RAS spectrum at 2.5 eV with the 2.6-eV optical transition, which is derived from a filled Sn-Si backbond state and an empty Sn-Sn dangling-bond state. The broad negative structure observed from 2.6 to 4.0 eV may indicate a contribution from the S_3 filled state to the empty Sn-Sn dangling-bond state.

3.1.5 ML coverages and above: The (5×1) phase

From Fig. 3(b), it can be seen that a significant increase in optical anisotropy is observed after deposition of 1.5 ML of Sn followed by annealing. LEED shows a predominantly

single-domain (5×1) phase for this RAS line shape, indicating that the single-domain nature of the clean surface is preserved through Sn deposition [see Fig. 4(d)]. The RAS line shape is considerably different from the lower-coverage Sn-induced phases, being dominated by a large and positive anisotropy feature centered at 1.8 eV. However, above this energy, similarities to the lower-coverage phases are evident, with a broad trough now shifted up in energy with respect to the $c(8\times 4)$ phase and peaking at 2.9 eV.

In order to shed light on the origin of these peaks, we again refer to the electronic properties for this surface as outlined by Pedio *et al.*^{8,9} From the ARUPS data, only one filled state near 1.4 eV with a dispersion of approximately ± 0.4 eV and one empty state at 2.5 eV are observed. With IPES, some intensity at the Fermi level is observed, which is indicative of metallicity. Assuming the correct symmetry of these states, a RAS feature may be expected in the 2.0–3.0 eV region, which could explain the observation of a trough at 2.8 eV. A transition from the filled state to the metallic states near the Fermi level may also explain the presence of the large 1.8 eV peak.

As the structure shows evidence for metallicity and also contains apparent chains, we compare this RAS line shape with the line shapes of other such systems grown on Si surfaces. It has been shown that the (5×2)-Au and (4×1)-In structures formed on a single-domain Si(111) surface through deposition of 0.2–0.5 ML of Au and 0.75–1.0 ML of In, respectively, display a strong optical anisotropy, the RAS signal being larger for light polarized perpendicular to the apparent chain lengths.^{30,31} Evidence of one-dimensional metallicity was shown on both surfaces through angle-resolved photoemission measurements. Accurate structural models for these reconstructions have still not been fully developed and so the origin of the optical anisotropy has not been associated specifically with any surface atomic features. However, for the (5×1)-Sn surface, we find that the larger reflectivity for light polarized perpendicular to the apparent chains is dependent on the formation of second-layer Sn-Sn dimers, which must also be responsible for making the (5×1)-Sn surface metallic. Therefore, as a general comment, it seems that any apparent chainlike structures with a metallic character produce a large RAS intensity *perpendicular* to the apparent chains, which is independent of the species used. Electronic confinement perpendicular to the apparent chain length, giving rise to discrete and highly populated surface states in this direction, may explain this experimental observation.³¹

Upon deposition of more than 1.5 ML of Sn followed by annealing, the anisotropy in the region of the 1.8-eV peak decreases [see Fig. 3(b)]. This is consistent with the 1.8-eV peak being related specifically to the (5×1) reconstruction and not to the formation of directional α -Sn islands, which are known to start forming above 1.5-ML coverage.³² Further evidence for this argument comes from annealing of the (5×1) phase to higher temperatures, in order to promote the desorption of Sn. After annealing, the lower Sn coverage induced $c(8\times 4)$ phase is observed using LEED. This is accompanied by loss of the 1.8-eV feature. Further deposition and annealing reestablishes the (5×1) LEED pattern and the

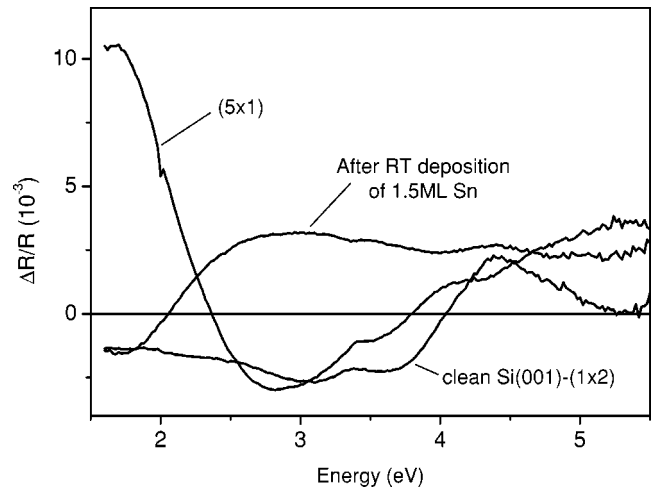


FIG. 6. RAS spectra of clean Si(001)-(1 \times 2), the (1 \times 1) surface formed after deposition of 1.5 ML of Sn at room temperature, and the (5 \times 1) phase formed after annealing.

RAS peak at 1.8 eV. Hence, the 1.8-eV peak is a clear fingerprint of the (5×1) phase.

C. The (5×1) phase: Room temperature versus annealed structure

Figure 6 shows the RAS spectra when 1.5 ML of Sn is deposited onto the clean vicinal Si(001) sample, along with the spectrum for the (5×1) phase obtained after annealing. Both spectra represent the largest RAS signals obtained for the room-temperature deposited and annealed surface, respectively. As the (5×1) reconstruction obtained after annealing is known to saturate in the region of 1.5-ML Sn coverage,¹⁰ it is clear that upon annealing the as-deposited sample to 570 °C/2 min does not induce any Sn desorption. Supporting evidence comes through monitoring the desorption of Sn from the (5×1) reconstruction using RAS set to an energy of 1.8 eV. Here, the amplitude of the anisotropy undergoes a sharp change once the sample is annealed above 740 °C (see Fig. 7). Once the sample had cooled after this anneal, the characteristic line shape of a clean stepped Si(001) surface is regained, indicating that the sharp change in anisotropy is caused by the desorption of Sn. Hence, Sn desorption occurs at 740 °C, which is significantly higher than the annealing temperature used.

Ignoring the trough in the region of 2.8 eV obtained for the (5×1) structure, it can be seen from Fig. 6 that both spectra bear a striking similarity to one another, the only differences being a difference in sign and amplitude. This seems surprising as, for room-temperature growth and after saturation of the (2×2) phase at 0.5 ML (see Sec. III A), additional Sn is reported to commence formation of a second layer, while at a coverage of 1.5 ML, it appeared probable that some third-layer Sn also existed.²³ After deposition of 1.5 ML, we observe a diffuse (1 \times 1) LEED pattern. For the annealed case, a second Sn layer does not start forming until the $c(8\times 4)$ structure is saturated at near 1-ML coverage. Additional Sn commences formation of a second layer and when an extra 0.5-ML of Sn has been deposited, a sharp

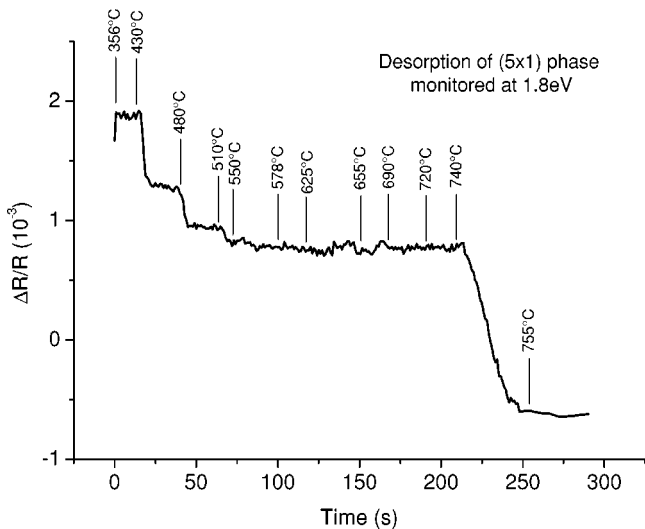


FIG. 7. RAS dynamic scan taken at 1.8 eV during annealing of the (5×1) reconstruction to induce Sn desorption.

(5×1) LEED pattern is observed. Hence, considering the differences in preparation, it may appear that the similarity of both RAS traces is merely coincidental.

In the detailed STM paper of Glueckstein *et al.*²³ for room-temperature growth of Sn on Si(001), a striped phase with local (2×5) ordering is described for Sn coverage in the region of 1 ML.²³ Surprisingly, this (2×5) ordering was found to have the same periodicity, number of maxima, and bias dependence as the STM data of Baski *et al.* for the (5×1) phase.¹⁰ Furthermore, the registration of the Sn maxima for the second layer, which starts to form near 1 ML for the annealed surface and near 0.5 ML for the room-temperature deposited sample, with respect to the underlying Si surface, was found to be the same.

Our RAS data support this similarity in local ordering in both cases. In order to interpret these data in the context of the findings of Glueckstein *et al.*,²³ we note first of all that RAS is well known to be sensitive to the orientation of surface features, changing sign depending on the orientation of a particular feature.¹⁶ Hence, the change in sign that is observed in this work may be related to orientation differences within the adsorbed Sn layer. From the discussion of the (5×1) phase in the preceding section, we pointed out that the particular stability of this phase was likely to be related to the formation of second-layer Sn dimers between unbroken Sn dimers of the first-layer $c(8 \times 4)$ structure, which at a second-layer coverage of 0.5 ML would have the effect of reducing the number of dangling bonds in the system by half,

thus reducing the surface energy. The orientation of second-layer Sn dimers is unclear, but the Sn dimers of the underlying Sn layer are known to be oriented in the $[\bar{1}10]$ direction [see Fig. 5(b) for a model of the $c(8 \times 4)$ structure]. For Sn deposition without annealing, as outlined above, the second Sn layer starts forming above saturation of the (2×2) phase at 0.5-ML coverage. Assuming the parallel Sn dimer model for the (2×2) structure [see Fig. 2(b)], the Sn dimers are also oriented in the $[\bar{1}10]$ direction. Therefore, as we detect a different RAS sign for the (5×1) surface and its room-temperature counterpart, second-layer Sn dimers must be responsible as the first-layer Sn dimers are oriented in the same direction. Hence, the second-layer Sn dimers must be oriented in orthogonal directions on both surfaces despite their similar appearance on the STM images. If this interpretation of the RAS spectra in Fig. 6 is correct, then the presence of steps plays a minor role in the overall anisotropy observed for these structures.

IV. CONCLUSIONS

In this work, we have applied RAS and LEED to the Sn/Si(001) system. We have shown that after room-temperature deposition, considerable changes occur in the RAS signal. A (2×2) LEED pattern is observed for a Sn coverage of 0.5 ML, its presence stabilized by the narrow terraces of the vicinal sample used. Once annealed, the $c(4 \times 4)$, (6×2) , $c(8 \times 4)$, and (5×1) reconstructions are observed with increasing Sn coverage using LEED. The RAS line shapes for the former three reconstructions are similar but show subtle differences in the 2–3-eV energy range, which is related to a gradual change of Sn-Si into Sn-Sn dimers on the surface with increasing coverage up to 1 ML. The RAS line shape for the (5×1) reconstruction formed at 1.5-ML coverage displays a significant anisotropy near 1.8 eV. The similarity between this and the line shape for a room-temperature Sn-induced structure points to a Sn-Sn dimer origin for both line shapes. Higher Sn coverages lead to island formation, reducing the intensity of the RAS signal and ruling out the formation of oriented α -Sn islands or facing as the origin of the 1.8-eV peak.

ACKNOWLEDGMENTS

A. Astropekakis wishes to thank I. Simitzis for his encouragement and the financial support of the N.T.U.A. EU program “ERASMUS.” J. R. Power acknowledges support from the Alexander von Humboldt Foundation.

*Corresponding author. Present address: Infineon Technologies, TD L, Königsbrücker Strasse 180, D-01076 Dresden, Germany.

¹D. H. Rich, T. Miller, A. Samsavar, H. F. Hin, and T.-C. Chiang, Phys. Rev. B **37**, 10 221 (1988).

²G. Le Lay and K. Hricovini, Phys. Rev. Lett. **65**, 807 (1990).

³C. L. Griffiths, H. T. Anyele, C. C. Matthai, A. A. Cafolla, and R. H. Williams, J. Vac. Sci. Technol. B **11**, 1559 (1993).

⁴X. W. Lin, Z. Liliental-Weber, J. Washburn, E. R. Weber, A.

Sasaki, A. Wakahara, and T. Hasegawa, J. Vac. Sci. Technol. B **13**, 1805 (1995).

⁵X. W. Lin, Z. Liliental-Weber, J. Washburn, E. R. Weber, A. Sasaki, A. Wakahara, and T. Hasegawa, Phys. Rev. B **52**, 16 581 (1995).

⁶N. Kuwata, T. Asai, K. Kimura, and M. Mannami, Surf. Sci. **143**, L393 (1984).

⁷K. Ueda, K. Kinoshita, and M. Mannami, Surf. Sci. **145**, 261

- (1984).
- ⁸M. Pedio, V. Ghisalberti, C. Ottaviani, C. Capozzi, F. Lama, C. Quaresima, and P. Perfetti, *Surf. Sci.* **303**, 153 (1994).
- ⁹M. Pedio and C. Cricenti, *Surf. Sci.* **374**, 251 (1997).
- ¹⁰A. A. Baski, C. F. Quate, and J. Nogami, *Phys. Rev. B* **44**, 11 167 (1991).
- ¹¹P. F. Lyman and M. J. Bedzyk, *Surf. Sci.* **371**, 307 (1997).
- ¹²D. E. Aspnes, J. P. Harbison, A. A. Studna, and L. T. Florez, *J. Vac. Sci. Technol. A* **6**, 1327 (1988).
- ¹³T. Yasuda, L. Mantese, U. Rossow, and D. E. Aspens, *Phys. Rev. Lett.* **74**, 3431 (1995).
- ¹⁴L. Kipp, D. K. Biegelsen, J. E. Northrup, L.-E. Swartz, and R. D. Bringans, *Phys. Rev. Lett.* **76**, 2810 (1996).
- ¹⁵A. I. Shkrebtii, N. Esser, W. Richter, W. G. Schmidt, F. Bechstedt, A. Kley, B. O. Fimland, and R. Del Sole, *Phys. Rev. Lett.* **81**, 721 (1998).
- ¹⁶J. R. Power, P. Weightman, S. Bose, A. I. Shkrebtii, and R. Del Sole, *Phys. Rev. Lett.* **80**, 3133 (1998).
- ¹⁷K. Ploska, J.-T. Zettler, W. Richter, J. Jönsson, F. Reinhardt, J. Rumberg, M. Pristovsek, M. Zorn, D. Westwood, and R. H. Williams, *J. Cryst. Growth* **145**, 44 (1994).
- ¹⁸M. Zorn, P. Kurpas, A. I. Shkrebtii, B. Junno, A. Bhattacharya, K. Knorr, M. Weyers, L. Samuelson, J. T. Zettler, and W. Richter, *Phys. Rev. B* **60**, 8185 (1999).
- ¹⁹A. I. Shkrebtii and R. Del Sole, *Phys. Rev. Lett.* **70**, 2645 (1993).
- ²⁰K. Fleischer (unpublished).
- ²¹W. Richter, *Philos. Trans. R. Soc. London, Ser. A* **344**, 453 (1993).
- ²²S. G. Jaloviar, J.-L. Lin, F. Liu, V. Zielasek, L. McCaughan, and M. G. Lagally, *Phys. Rev. Lett.* **82**, 791 (1999).
- ²³J. C. Glueckstein, M. M. R. Evans, and J. Nogami, *Surf. Sci.* **415**, 80 (1998).
- ²⁴J. Nogami, A. A. Baski, and C. F. Quate, *Phys. Rev. B* **44**, 1415 (1991).
- ²⁵Y. Qian, M. J. Bedzyk, and S. Tang, *Phys. Rev. Lett.* **73**, 1521 (1994).
- ²⁶H. Itoh, H. Tanabe, and D. Winau, *J. Vac. Sci. Technol. B* **12**, 2086 (1994).
- ²⁷D. J. Chadi, *Phys. Rev. Lett.* **59**, 1691 (1987).
- ²⁸E. Pehlke and J. Tersoff, *Phys. Rev. Lett.* **67**, 465 (1991).
- ²⁹C. S. Chang, Y. M. Huang, and T. T. Tsong, *Phys. Rev. Lett.* **77**, 2021 (1996).
- ³⁰J. R. Power, P. Weightman, and J. D. O'Mahony, *Phys. Rev. B* **56**, 3587 (1997).
- ³¹F. Pedreschi, J. D. O'Mahony, P. Weightman, and J. R. Power, *Appl. Phys. Lett.* **73**, 2152 (1998).
- ³²L. Li, Y. Wei, and I. S. Tsong, *J. Vac. Sci. Technol. A* **13**, 1473 (1995).